https://doi.org/10.5194/egusphere-2024-3363
Preprint. Discussion started: 13 December 2024

A New Technique to Retrieve Aerosol Vertical Profiles Using Micropulse Lidar and Ground-based Aerosol Measurements

Bo Chen[1], Seth A. Thompson[1], Brianna H. Matthews[1,2], Milind Sharma[1], Ron Li[1], Christopher J. Nowotarski[1], Anita D. Rapp[1], and Sarah D. Brooks[1]

[1]Atmospheric Sciences Department, Texas A&M University, College Station, 77843, United States
[2]now at Savannah River National Laboratory, Aiken, South Carolina, 29808, United States

Correspondence to: Sarah D. Brooks (sbrooks@tamu.edu)

Abstract.

Accurately characterizing the vertical distribution of aerosols and their cloud-forming properties is crucial for understanding aerosol-cloud interactions and their impact on climate. This study presents a novel technique for retrieving vertical profiles of aerosols, cloud condensation nuclei (CCN), and ice nucleating particles (INPs) by combining micropulse lidar, radiosonde, and ground-based aerosol measurements. Herein, the technique is applied to data collected by our team at Texas A&M University during the Tracking Aerosol Convection Interactions ExpeRiment (TRACER) campaign. Aerosol size distribution and CCN counter data are used to estimate the value of the aerosol hygroscopicity parameter, κ. The derived κ, together with Mie scattering theory and the relative humidity profiles from the radiosonde, are then used to estimate how much the aerosols have grown at each altitude. This estimate is applied inversely to the aerosol backscatter coefficient profile to produce a dry aerosol backscatter coefficient profile. The dry aerosol backscatter coefficient profile is used to linearly scale surface measurements of aerosol, CCN, and INP concentrations. Combining lidar and ground-based aerosol measurements reduces the assumptions typically needed in lidar-based aerosol retrievals, resulting in a more accurate representation of vertical distributions of aerosol properties. The method could be readily applied to measurements in future field campaigns.

https://doi.org/10.5194/egusphere-2024-3363
Preprint. Discussion started: 13 December 2024

1 Introduction

The interaction between aerosols and clouds introduces significant uncertainties in estimating aerosol indirect radiative forcing, a critical factor in predicting future climate scenarios (Seinfeld et al., 2016). Aerosols can facilitate the formation of cloud water droplets and cloud ice particles by acting as cloud condensation nuclei (CCN) and ice nucleating particles (INPs), respectively. Consequently, changes in aerosol concentrations could influence a number of convective cloud properties and processes (Tao et al., 2012; Fan et al., 2016). For example, increased CCN concentrations could result in smaller cloud droplet sizes, suppress local precipitation in warm-phase clouds, and extend cloud lifetimes (Twomey, 1977; Albrecht, 1989). Some studies have suggested that an increased concentration of ultrafine aerosol particles (smaller than 50 nm) leads to enhanced condensational heating from additional water vapor condensation. Since this process invigorates the updraft intensity, it has been referred to as warm-phase invigoration (Fan et al., 2007; Fan et al., 2018; Lebo and Seinfeld, 2011). Other studies have focused on cold-phase invigoration of updrafts, a process in which cloud water freezes, releasing latent heat and subsequently increasing the buoyancy of air parcels (Andreae et al., 2004; Rosenfeld et al., 2008). At present, the extent and significance of aerosol-induced invigoration effects are under debate (Lebo, 2018; Igel and Van Den Heever, 2021; Varble et al., 2023). Addressing these uncertainties requires a deeper understanding of the microphysical processes involved (Jensen, 2023). One of the key gaps in our current understanding of aerosol-cloud interactions is the vertical distribution of aerosols, CCN, and INPs in the cloud environment.

The knowledge of the aerosol vertical distribution is important for assessing aerosol-cloud interactions (Rosenfeld et al., 2014; Lin et al., 2023). Modeling studies have shown evidence that the altitude of aerosol significantly influences their impact on cloud formation and deep convection (Marinescu et al., 2017; Lebo, 2014; Zhang et al., 2021). However, in most long-term field campaigns, aerosol, CCN, and INP measurements are only made at ground-based sampling stations (Schmale et al., 2018; Pöhlker et al., 2016; Perkins et al., 2022). By comparison, airborne in-situ measurements which provide observations of CCN and INP at the cloud level are generally shorter in duration (Stith et al., 2009; Dadashazar et al., 2022; Raes et al., 2000). Thus, retrievals from ground-based lidar observations, which can operate

https://doi.org/10.5194/egusphere-2024-3363
Preprint. Discussion started: 13 December 2024

continuously over extended periods to quantitatively assess vertical profiles aerosol properties, represent a highly valuable method.

Lidars detect range-resolved properties of aerosols and cloud particles by emitting laser pulses and measuring the backscattered light. Lidar measurements can be used to retrieve bulk aerosol optical properties, including the aerosol backscatter coefficient, extinction coefficient, and depolarization ratio. These aerosol optical properties are influenced by various aerosol properties, including size distribution, shape, chemical composition, and mixing state (Brooks et al., 2004b; Titos et al., 2016; Yao et al., 2022). While the same intrinsic properties drive microphysical properties, the relationship between the lidar observations and the concentration of cloud-forming aerosol is not straightforward. Most CCN are found within the Aitken (typically between 0.01 to 0.1 μm) and accumulation (typically between 0.1 to 1 μm) mode aerosols, but lidar observations at visible wavelengths are most sensitive to the accumulation and coarse (typically greater than 1 μm) mode aerosols (Shinozuka et al., 2015; Kapustin et al., 2006). In addition, aerosol hygroscopic growth due to increased humidity increases the aerosol backscatter coefficient without affecting the CCN concentration (Shinozuka et al., 2015; Liu and Li, 2014). As for INP, it has been shown that larger aerosols are more likely to be INP, particularly those with a diameter exceeding 500 nm (Demott et al., 2010). Individual aerosols in this size range backscatter light effectively, but less than 1 in 10^5 particles in the atmosphere can act as INPs (Demott et al., 2010). Thus, INPs contribute little to the measured bulk aerosol optical signals. Consequently, it is necessary to employ assumptions or complementary aerosol measurements when estimating cloud-forming aerosol concentration from remote sensing measurements.

Studies have adopted different approaches when using lidar measurements to retrieve the CCN concentration vertical profile (Lv et al., 2018; Mamouri and Ansmann, 2016; Ansmann et al., 2021; Ghan et al., 2006; Ghan and Collins, 2004; Lenhardt et al., 2023). The first approach involves using multi-wavelength lidar to retrieve aerosol concentrations by classifying them into three types (urban, biomass burning, and dust) and then using the prescribed hygroscopicity parameter of each aerosol type to estimate the CCN concentration (Lv et al., 2018). This approach requires an advanced multiwavelength lidar, such

https://doi.org/10.5194/egusphere-2024-3363
Preprint. Discussion started: 13 December 2024

as the Multiwavelength High Spectral Resolution Lidar (HSRL-2) or the multiwavelength Raman lidar (Müller et al., 2011; Müller et al., 2014). Another approach relies on an empirical relation between the aerosol extinction coefficient and aerosol concentrations derived from the Aerosol Robotic Network (AERONET) to convert backscatter into aerosol concentration profile. A CCN parameterization scheme based on the empirical relation of aerosol and CCN concentration of each aerosol type is applied to the aerosol concentration profile to produce the CCN concentration profile (Mamouri and Ansmann, 2016; Ansmann et al., 2021). Each of these approaches strongly relies on assumed aerosol composition, shape, and refractive index used in the lidar retrieval and CCN parameterizations. Consequently, they may fail to capture the complex conditions of atmospheric aerosols, thus limiting the precision of CCN estimations.

The third approach to determining CCN concentration using lidar is to directly scale ground-based CCN concentration measurement with the lidar-measured extinction or backscatter profile, first proposed by Ghan and Collins (2004). This approach assumes that the aerosol composition and size distribution remain relatively constant with altitude. Ghan and Collins (2004) used the humidification factor (hereby referred to as the lidar hygroscopic growth correction factor), defined as the dependence of aerosol extinction or backscatter on relative humidity (RH), to convert the observed extinction and backscatter coefficients to their dry counterparts. Ghan and Collins (2004) found that CCN concentrations at smaller supersaturations correlate more strongly with dry backscatter and are less impacted by height variations in aerosol size distribution than at higher supersaturations. Ghan et al. (2006) later validated this approach, showing that the correlation between lidar-derived and in situ CCN is influenced by supersaturation, aerosol uniformity with height, and lidar retrieval accuracy. This method has been applied in a routine CCN profile data product based on a Raman lidar (Kulkarni et al., 2023). Following a similar approach, Lenhardt et al. (2023) compared in-situ CCN and airborne HSRL-2 measurements in the southeast Atlantic. Their results show that CCN concentration at 0.3% supersaturation in dry ambient conditions strongly correlates with the HSRL-2 measured extinction and backscatter. Collectively, these studies demonstrate the strong potential of lidar observations for accurately retrieving CCN profiles.

https://doi.org/10.5194/egusphere-2024-3363
Preprint. Discussion started: 13 December 2024

Compared to the lidar retrievals of CCN, fewer studies have focused on INP retrievals using lidar data. Studies have combined INP parameterization with lidar measurement to retrieve INP concentration profiles (Mamouri and Ansmann, 2016; Marinou et al., 2019; Ansmann et al., 2021). A number of INP parameterization schemes based on previous ice nucleation measurements are available in the literature for total global aerosols of unspecified composition (Demott et al., 2010), dust (Ullrich et al., 2017; Demott et al., 2015; Niemand et al., 2012; Steinke et al., 2015), soot aerosols (Ullrich et al., 2017), biological aerosols (Tobo et al., 2013), and organics (Wang and Knopf, 2011). Generalized aerosol type and composition assumptions must be made when using these INP parameterizations, which depend on past measurements from other locations or lab experiments. In contrast, lidar retrievals based on simultaneous ground-based INP measurements would provide a more realistic estimate of ice nucleation. We propose that analogous to CCN profile retrieval, INP concentration measured at the surface can be linearly scaled by the dry backscatter coefficient profile derived from lidar measurements to create an estimate of the INP vertical profile.

Despite advancements in understanding aerosol and cloud interaction, significant uncertainties remain in accurately characterizing aerosol vertical distribution and their impact on cloud processes. Existing models and observations often rely on assumptions that can introduce biases, highlighting the need for dedicated field campaigns that provide comprehensive measurements to fill these knowledge gaps. The Tracking Aerosol Convection Interactions ExpeRiment (TRACER) campaign focused on understanding aerosol-cloud/convection interaction in the Houston area in the summer and fall of 2022 (Jensen, 2023). In this study, we use the micropulse lidar and ground-based aerosol measurements we collected during the TRACER campaign to develop a purely measurement-based approach to retrieve the aerosol, CCN, and INP vertical profiles. The ground-based aerosol measurements include aerosol size distribution, CCN, and INP measurements. By leveraging observations to minimize assumptions in the retrieval process, this approach is expected to represent aerosol properties and their vertical distribution accurately.

https://doi.org/10.5194/egusphere-2024-3363
Preprint. Discussion started: 13 December 2024

2 Methodology

2.1 Overview of TRACER Field Campaign

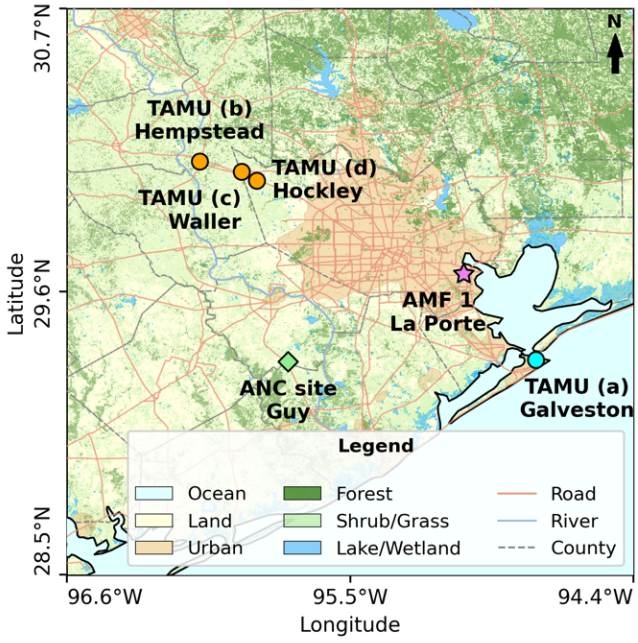

Figure 1 TRACER Campaign Sampling Locations in the Houston metropolitan area, Texas. The Texas A&M University sampling sites are marked with circles, the ARM AMF1 site is marked with a star, and the ARM ancillary site is marked with a diamond. Map created using Natural Earth shapefiles, LandFire 2022 vegetation data, and USA Detailed Water Bodies data.

The U.S. Department of Energy TRACER field campaign was conducted from October 2021 through September 2022 in the Houston metropolitan area, with an intensive observation period (IOP) from June 2022 to September 2022 at sites shown in Figure 1. The First Atmospheric Radiation Measurement (ARM) Mobile Facility (AMF-1) was deployed at La Porte, Texas throughout the campaign. On enhanced operations days during the IOP period, the Texas A&M University (TAMU) Rapid Onsite Atmospheric Measurements Van (ROAM-V) was deployed at Seawolf Park, a coastal site in Galveston, Texas, and several inland sites (Rapp et al., 2024). An overview of the TAMU TRACER campaign payload, deployment strategy, and available measurements is provided by Rapp et al. (2024). Both AMF1 and ROAM-V collected similar ground-based aerosol measurements, radiosonde data, and ground-based lidar

https://doi.org/10.5194/egusphere-2024-3363
Preprint. Discussion started: 13 December 2024

profiles, as described in Table 1. The lidar retrieval method described below was initially developed based on the ROAM-V instrumentation but is also applied to the observations at the AMF-1 site during TRACER. By extension, this method could be used in other future campaigns with a similar instrumentation configuration.

155

Table 1. A list of data and instruments used in this study.

Measurements	**TAMU ROAM-V**	**ARM AMF-1**
Aerosol Extinction and backscatter profile	MiniMPL (Brooks and Chen, 2023)	MPL (Muradyan, 2021)
Pressure, temperature, and relative humidity profile	iMet-4 (Sharma et al., 2023)	Vaisala RS41 (Keeler, 2021)
Ground-based aerosol measurements		
Aerosol concentration and size distribution	SMPS, POPs (Chen et al., 2024)	SMPS, APS (Shilling, 2021)
CCN concentration	CCN-100 (Thompson, 2023)	CCN-200 (Koontz, 2021)
INP concentration	DRUM impactor and TAMU droplet freezing array (Brooks and Thompson, 2023)	

Figure 2 provides an overview of the retrieval routine for aerosol, CCN, and INP profiles using the TRACER campaign data. The routine is summarized here. First, we used lidar and radiosonde data to
160 determine the vertical profile of the cloud-free aerosol backscatter coefficient. Next, the aerosol size distribution and concentration collected with Scanning Mobility Particle Sizer (SMPS), Portable Optical Particle Spectrometer (POPS), and CCN counter are used to estimate the lidar hygroscopic growth correction factor, f(RH), which is the ratio of aerosol optical properties at a given relative humidity to those at dry conditions. f(RH) is then used to convert the aerosol backscatter coefficient profile to a dry
165 aerosol backscatter coefficient profile. This dry aerosol backscatter coefficient profile is used to linearly scale the surface aerosol concentration, CCN concentration, and INP concentration measurements.

https://doi.org/10.5194/egusphere-2024-3363
Preprint. Discussion started: 13 December 2024

Below, we discuss details of each step of the retrieval process with TAMU ROAM-V data collected on 28 August 2022 in Galveston, Texas, as an example.

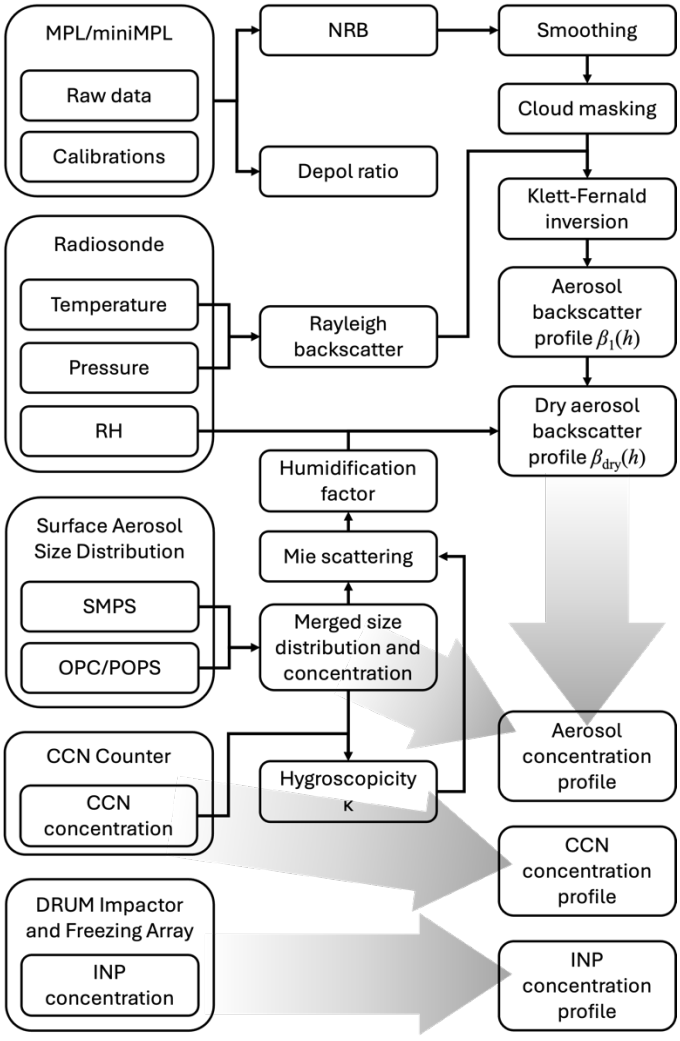

Figure 2 Overview of the aerosol, CCN, and INP profile retrieval routine.

2.2 Micropulse Lidar Measurement and Inversion of the Lidar Equation

The mini micropulse lidar (MiniMPL, Droplet Measurement Technologies, Inc.) is a 532-nm backscatter and depolarization lidar (Campbell et al., 2002; Flynna et al., 2007; Welton and Campbell, 2002). The MiniMPL uses a vertical resolution of 15 m and a temporal resolution of 1 min in the TRACER campaign. The Normalized Relative Backscatter (NRB), also known as the attenuated backscatter, is derived from

https://doi.org/10.5194/egusphere-2024-3363
Preprint. Discussion started: 13 December 2024

the raw backscattered lidar signal after standard background, afterpulse, deadtime, and overlap corrections are performed. Details of the corrections are presented in the supporting information (Equation S1-4). An example of an NRB time series collected by the MiniMPL is shown in Figure 3.

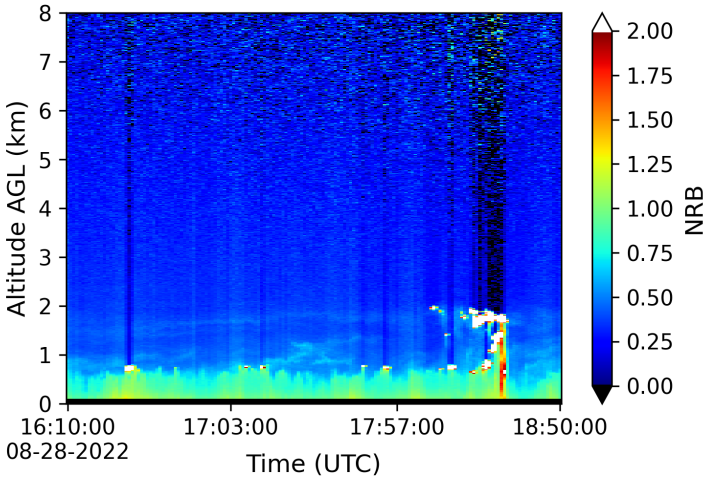

Figure 3 Normalized relative backscatter time series collected on August 28, 2022, with MiniMPL in Galveston, Texas.

NRB can be expressed as,

$$NRB(R) = C[\beta_1(R) + \beta_2(R)]T_1^2(R)T_2^2(R) \quad (1)$$

Where R is the range, C is the lidar calibration constant, β_1 and β_2 represent the backscatter coefficient of aerosol and air molecules, respectively; T_1 and T_2 represent the transmittance of aerosol and air molecules, respectively. After correcting the raw lidar data to produce the NRB profile, data filtering and smoothing are applied to the NRB profile. First, a continuous wavelet transform based algorithm is used to create a cloud mask, filtering out periods of data with cloud signal peaks in the NRB profile that compromise the quality of aerosol retrieval (Du et al., 2006). Because the MiniMPL collects measurements near the peak of the solar spectrum, observations can have a considerable amount of background noise during daytime measurements (Campbell et al., 2002). The NRB profiles of cloud-free columns, typically between about one to two hours before and after the radiosonde launch time, are time-averaged to improve signal-to-

https://doi.org/10.5194/egusphere-2024-3363
Preprint. Discussion started: 13 December 2024

noise ratio. This averaged NRB profile is further normalized by the average NRB value of the lowest range bin. In addition, the NRB profile above 4.5 km is smoothed using the NeighBlock denoising algorithm based on discrete wavelet transform to increase the stability of the retrieval process (Cai and Silverman, 2001). Similar wavelet transform techniques have been widely used in lidar applications for noise reduction and feature detection because the lidar signal exhibits a varying degree and frequency of noise at different ranges (Fang and Huang, 2004; Xie et al., 2017).

Next, a Fernald 2-component lidar inversion method is performed. This is a classic method for solving the lidar equation and retrieving aerosol backscatter profiles from the attenuated backscatter (Fernald et al., 1972; Klett, 1981; Fernald, 1984; Sasano et al., 1985). The lidar ratio (S), defined as the ratio of aerosol extinction coefficient to aerosol backscatter coefficient, is assumed to be constant with respect to range (R). Following the Fernald method, the sum of aerosol ($\beta_1(R)$) and molecular backscatter coefficient ($\beta_2(R)$) is expressed as:

$$\beta_1(R)+\beta_2(R)=\frac{\mathrm{NRB}(R)\cdot exp\left[-2(S_1-S_2)\int_{R_C}^{R}\beta_2(r)\mathrm{d}r\right]}{\frac{\mathrm{NRB}(R_C)}{\beta_1(R_C)+\beta_2(R_C)}-2S_1\int_{R_C}^{R}\mathrm{NRB}(r)\cdot exp\left[-2(S_1-S_2)\int_{R_C}^{r}\beta_2(r')\mathrm{d}r'\right]\mathrm{d}r} \quad (2)$$

The numerical form of Equation 2 used for the calculation is shown in supporting information (Equation S5). S_1 and S_2 in Equation 2 represent the lidar ratio of aerosol and air molecules, respectively. S_2 is approximated by the well-known constant $8\pi/3$ sr (Fernald, 1984). R_C is the calibration range selected at the far field, and usually, *a priori* information is needed to set the reference aerosol backscatter at the calibration range. At a wavelength of 532 nm, the aerosol lidar ratio typically ranges from 23±5 sr for clean marine aerosols, 44±9 for dust, 53±24 sr for clean continental aerosols, 55±22 sr for polluted dust, to 70±25 sr for polluted continental and smoke aerosols (Young et al., 2018). To account for the potential variability of the lidar ratio, we choose 20 and 90 sr as the lower and upper estimates of aerosol lidar ratio, respectively. The calibration range, R_C, was chosen to be 8 km AGL. At this range, we assume the

https://doi.org/10.5194/egusphere-2024-3363
Preprint. Discussion started: 13 December 2024

calibration scattering ratio (β_1(R)+β_2(R))/β_2(R), which is the ratio of the sum of aerosol and molecular backscatter coefficient and molecular backscatter coefficient, varies between 1.0 and 1.2.

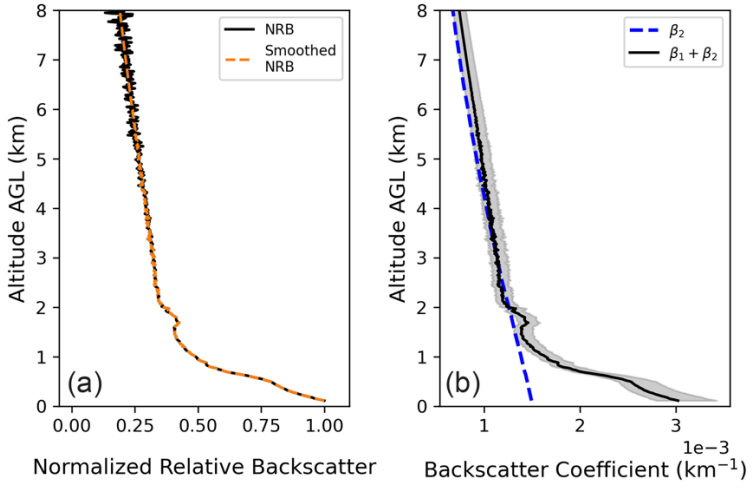

Figure 4 (a) Time-averaged Normalized Relative Backscatter (NRB) profile of MiniMPL from 16:10 to 18:50 UTC. The black line is the NRB profile normalized by the lowest level value; the orange dashed line represents smoothed NRB. (b) Rayleigh backscatter coefficient β_2 (dashed blue line) and total backscatter coefficient β_1+ β_2 (solid black line). The shaded region shows the uncertainty range of the retrieved total backscatter coefficient.

The Rayleigh backscatter $\beta_2(R)$ by gas phase molecules is calculated using the following equation (Gimmestad and Roberts, 2023).

$$\beta_2(R) = 1.39 \times \left[\frac{0.55\ \mu m}{\lambda}\right]^4 \times 10^{-6} \cdot \frac{288.15\ K}{1013.25\ hPa} \cdot \frac{P(R)}{T(R)} \quad (3)$$

$P(R)$ and $T(R)$ are pressure and temperature profiles measured by radiosondes launched during the TRACER campaign, and λ is the lidar wavelength, 532 nm. Finally, Equation 2 can be iteratively solved in a top-down approach, starting from the calibration range and working toward the surface. The aerosol backscatter coefficient profile can be calculated by subtracting the molecular backscatter coefficient profile from the total backscatter coefficient profile.

https://doi.org/10.5194/egusphere-2024-3363
Preprint. Discussion started: 13 December 2024

An example of NRB profile and backscatter coefficient profile inversion is shown in Figure 4. The cloud-free NRB profile of MiniMPL is time-averaged between 16:10 to 18:50 UTC at Sea Wolf Park on 28 August 2022. The Rayleigh backscatter coefficient profile, shown in blue dashed lines in Figure 4b, is calculated using data from the radiosonde launched around 17:30 UTC from the same site, and the total backscatter coefficient derived from the lidar inversion is shown in Figure 4b as a black solid line. The total backscatter coefficient profile closely follows the molecular backscatter coefficient profile 2 km AGL and above, which indicates that the backscatter coefficient is primarily influenced by molecular scattering at higher altitudes, with minimal contributions from aerosols.

The uncertainty in the total backscatter coefficient is assessed by systematically varying key parameters: the scattering ratio at the calibration height and the lidar ratio. The Fernald inversion process was applied 40 times to the same NRB profile, using 5 calibration scattering ratios (1.0 to 1.2) and 8 lidar ratios (20 to 90 sr), producing 40 backscatter coefficient profiles. The mean of these backscatter coefficient profiles can be considered as the best estimate, while the spread of these profiles from the maximum and minimum of these profiles represents the uncertainty interval. This systematic sensitivity analysis ensures that the retrieved aerosol backscatter profile accounts for potential variability in the lidar ratio and the scattering ratio, providing a more reliable estimate. The uncertainty range of the retrieved backscatter coefficient is shown in Figure 4b as the grey-shaded region.

https://doi.org/10.5194/egusphere-2024-3363
Preprint. Discussion started: 13 December 2024

2.3 Ground-based Aerosol Measurements

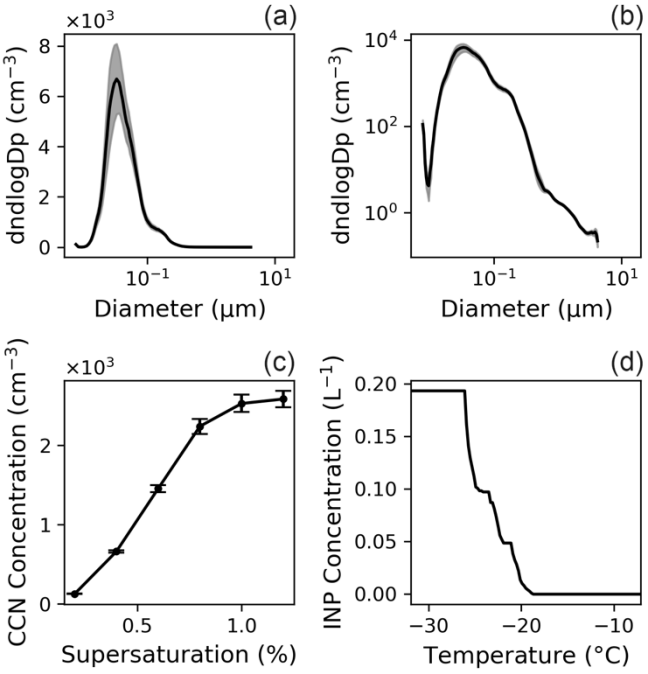

Figure 5 Time-averaged aerosol measurements were collected on 28 August 2022, from 16:10 to 18:50 UTC at the TAMU site in Galveston. (a) Time-averaged aerosol size distribution with a y-axis on a linear scale. The shaded area illustrates the standard error of the estimated mean. (b) Time-averaged aerosol size distribution with a y-axis on a log-log scale. (c) CCN spectra, where scatter points are time-averaged CCN concentrations at different supersaturations, and the standard error of the sample mean is illustrated as error bars. (d) INP spectra.

During the TRACER field campaign, the TAMU ROAM-V deployed a suite of surface aerosol measurements, which will be utilized in this analysis, as described in Table 1. The ROAM-V platform shares a heated and dried isokinetic inlet among the TSI Scanning Mobility Particle Sizer (SMPS), the Droplet Measurement Technologies CCN counter, and an additional GRIMM Condensation Particle Counter (CPC). Details of the ROAM-V instrument sampling setup for the TRACER campaign and the particle loss corrections are further described in Thompson et al. (2024).

https://doi.org/10.5194/egusphere-2024-3363
Preprint. Discussion started: 13 December 2024

Onboard ROAM-V, the SMPS measures the mobility diameter of aerosols between 7 and 305 nm, while the POPS measures the optical diameter of aerosols ranging from 125 to 3370 nm. Because the SMPS and POPS are based on different physical principles, a method was developed to merge their measured size distributions. Mie scattering theory is used to simulate the scattered signal by particles of various sizes detected by the POPS, generating a signal-size relation that depends on the aerosol effective refractive index. The POPS-measured aerosol sizes can be recalculated by adjusting the effective refractive index. The refractive index that minimizes the root mean square error of the overlapping size region between the POPS and SMPS distributions is then selected. The corresponding POPS size distribution is then merged with the SMPS size distribution by applying a weighted average over the overlapping region. The weights are determined by the Gaussian error function to ensure a smooth transition between the two distributions. The time average of the merged size distribution across the time-averaging period is used for further analysis. An example of the time-averaged aerosol size distribution measurement taken on 28 August 2022, from 16:10 to 18:50 UTC at Sea Wolf Park, is shown in Figure 5a and Figure 5b. The uncertainty of the aerosol size distribution is represented by two standard errors of the time-averaged aerosol size data to provide a 95% confidence interval for the time-averaged aerosol size distribution.

The CCN concentration spectra were measured with the CCN counter, which was set to supersaturations between 0.2% and 1.2% with intervals of 0.2%. The CCN counter was calibrated with size-selected ammonium sulfate particles. Similar to the merged aerosol size distribution, the time-averaged CCN spectra are calculated to represent the CCN concentration during the time-averaging period. An example of the average CCN measurement taken on 28 August 2022, from 16:10 to 18:50 UTC at the TAMU site in Galveston, is shown in Figure 5c. The two standard errors of CCN data are calculated to provide a 95% confidence interval for the time-averaged CCN concentration.

For ice nucleation measurements, size-resolved aerosol samples were collected using the Davis Rotating-drum Universal-size-cut Monitoring (DRUM) impactor in four size ranges: > 3 μm, 3 to 1.2 μm, 1.2 to 0.34 μm, and 0.34 to 0.15 μm, and analysed in the laboratory for ice nucleation measurements. Ice

https://doi.org/10.5194/egusphere-2024-3363
Preprint. Discussion started: 13 December 2024

nucleation measurements were conducted using the custom-built immersion freezing array used in our previous experiments (Lei et al., 2023; Thompson, 2024; Fornea et al., 2009), and described only briefly here. Aerosol impactor samples are washed off the impactor substrate into high purity UHPLC (ultra-high-pressure liquid chromatography) water. Then, 2-μL droplets of the sample water are subjected to 25 freeze-thaw cycles on the immersion freezing array. A digital camera is used to detect freezing events and identify ice nucleation temperatures by measuring the average brightness (or grayscale value) of the droplet pixels in an 8-bit image (which has 256 levels of grayscale value). This image-processing technique monitors changes in brightness to infer droplet freezing. The INP concentrations in the air are calculated using established methods (Vali, 1971).

2.4 Aerosol Hygroscopicity and Lidar Hygroscopic Growth Correction Factor

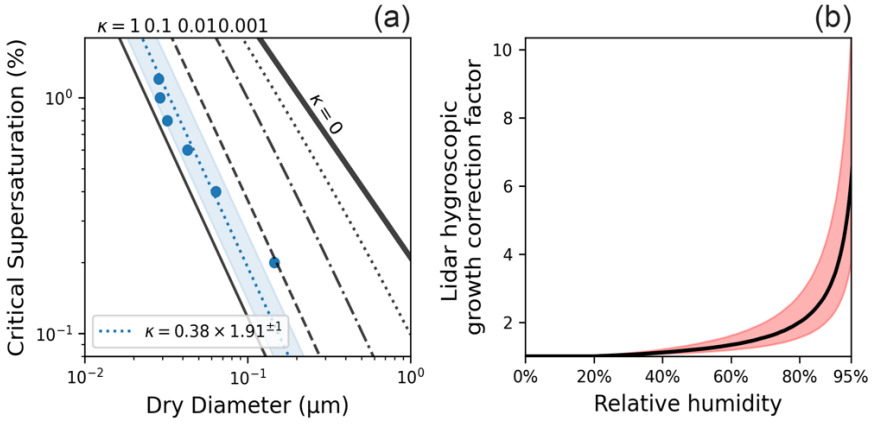

Figure 6 (a) Blue scattered points represent pairs of critical supersaturation and corresponding critical dry diameter derived from aerosol size distribution and CCN measurements. The blue dotted line represents the derived geometric mean of aerosol hygroscopicity *κ*, and the shaded region represents the one geometric standard deviation of *κ*. (b) Lidar hygroscopic growth correction factor as a function of relative humidity. The shaded area represents the uncertainties of derived κ.

Since water uptake by aerosols enlarges their size and increases backscattering without affecting aerosol concentration, it is not possible to accurately determine aerosol concentration from the aerosol backscatter

https://doi.org/10.5194/egusphere-2024-3363
Preprint. Discussion started: 13 December 2024

profile alone. It is important to convert the aerosol backscatter profile to the aerosol backscatter profile which would be observed under dry conditions prior to calculating aerosol, CCN, or INP concentrations. In past studies, the hygroscopicity or water uptake by aerosols, defined as the change in aerosol diameter at a given RH relative to its dry diameter, has been quantified by tandem differential mobility measurements (Brooks et al., 2004a; Tomlinson et al., 2007). Similarly, humidified nephelometers have been used to quantify changes in scattering by aerosol at increased relative humidities to scattering by dry aerosol, and the results have been used to interpret lidar backscatter observations (Kotchenruther et al., 1999; Ghan et al., 2006).

Here, we developed a new method that combines κ-Köhler theory with Mie theory to predict dry aerosol backscatter profiles from the observations at ambient RH. It is well-known that activated CCN are defined as those aerosols that have grown beyond the critical diameter required for spontaneous droplet growth. CCN activation occurs in a supersaturated environment. However, it has been demonstrated that for uniformly mixed soluble aerosol, CCN activation measurements can be used to predict hygroscopic growth of aerosol in subsaturated conditions as well (Petters and Kreidenweis, 2007). This widely used concept has become known as κ-Köhler theory (Petters and Kreidenweis, 2007).

Using κ-Köhler theory, CCN and aerosol size distribution measurements can be combined to predict an aerosol hygroscopicity parameter κ (kappa). The critical dry diameter $D_{p,c}$ is the size above which dry aerosols of a certain κ activate to form cloud droplets when exposed to a critical supersaturation SS_c. Following the work of Moore et al., 2011, $D_{p,c}$ satisfies the integral

$$N_{\mathrm{CCN}} = \int_{D_{p,c}}^{\infty} n_p(\log D_p)\, \mathrm{d}\log D_p \tag{4}$$

$n_p(\log D_p)$ is the measured aerosol size distribution in the form of $\mathrm{d}n\mathrm{d}\log D_p$, and N_{CCN} is the measured CCN concentration at a supersaturation level. $D_{p,c}$ can then be numerically solved. Since CCN concentration is measured at a few different supersaturations, multiple pairs of SS_c-$D_{p,c}$ values are

https://doi.org/10.5194/egusphere-2024-3363
Preprint. Discussion started: 13 December 2024

calculated, and an example of the SS_c-$D_{p,c}$ pairs is shown in Figure 6a. Each pair of SS_c-$D_{p,c}$ values can then be numerically solved using κ-Köhler theory to derive a κ value.

Following κ-Köhler theory, the saturation ratio S over an aqueous solution droplet with diameter D (also called wet diameter) can be expressed as

$$S(D) = \frac{D^3 - D_d^3}{D^3 - D_d^3(1-\kappa)} \exp\left(\frac{4\sigma_{\frac{s}{a}} M_w}{RT\rho_w D}\right) \quad (5)$$

D_d is the dry diameter of the particle. κ is the hygroscopicity parameter. $\sigma_{s/a}$ is the surface tension of the air-water interface. M_w is the molar mass of water. R is the universal gas constant. T is the temperature evaluated at 298.15 K. ρ_w is the density of water. The κ-Köhler equation relates saturation ratio to particle size, and the supersaturation at the peak indicates the activation point of the particle as a CCN. A numerical function was constructed to find the supersaturation at the peak of the κ-Köhler equation using binary search, with the particle dry diameter and κ as input parameters. Thus, the problem becomes finding the κ corresponding to a given $D_{p,c}$, to match a specific SS_c as the output. The κ is then numerically determined using a root-finding method to match the measured SS_c-$D_{p,c}$ pairs.

Since κ can be considered as log-normally distributed (Su et al., 2010), the geometric mean and geometric standard deviation can be calculated to represent the average value and the variability of κ for the bulk aerosol composition. An example of the geometric mean and geometric standard deviation of κ is also shown in Figure 6a. The variation in κ values at different supersaturations can be attributed to uncertainties in measurements and the differences in the aerosol chemical composition and mixing state across various sizes. Subsequently, the aerosol size growth is predicted by numerically solving for the wet aerosol diameter at a discrete series of RH values (Petters and Kreidenweis, 2007).

Once the aerosol size is known as a function of RH, the Mie scattering theory is then used to calculate the aerosol extinction coefficient at each RH value. The refractive index for dry aerosol is assumed to be

https://doi.org/10.5194/egusphere-2024-3363
Preprint. Discussion started: 13 December 2024

1.45-0i based on values for dry ammonium sulfate at 532 nm (Cotterell et al., 2017). The refractive index of aerosol at each RH is calculated as the volume-weighted average of the dry aerosol refractive index and that of water. During the field campaign, aerosol size distribution measurements are collected at RH levels below 30%, where aerosols are typically considered dry, based on the efflorescence RH of background ammonium sulfate (Onasch et al., 1999). Therefore, a lidar hygroscopic growth correction factor f(RH) can then be calculated as:

$$f(RH) = \begin{cases} \dfrac{\sigma(RH)}{\sigma(30\%)} & RH > 30\% \\ 1 & RH \leq 30\% \end{cases} \quad (6)$$

The extinction coefficient σ, rather than the backscatter coefficient, is used in the Mie scattering calculation. This is convenient since we already assumed a linear relation between backscatter and extinction in the lidar inversion, and it is justifiable based on the work on Ghan and Collins (2004) in which the influence of RH on backscatter and extinction were shown to be similar. In addition, we assume a perfect internally mixed aerosol distribution, and we apply the same κ across all aerosol sizes when predicting aerosol size growth at different RH. To account for the uncertainty of κ, we calculate the f(RH) using the geometric mean κ and its value at one geometric standard deviation interval. The f(RH) calculated using the κ values in Figure 6a is shown in Figure 6b. The solid black line represents the f(RH) calculated using the geometric mean κ, and the shaded region represents the f(RH) uncertainty calculated using one geometric standard deviation interval of κ. The calculated f(RH) is further interpolated using a cubic spline to calculate f(RH) at any RH value.

https://doi.org/10.5194/egusphere-2024-3363
Preprint. Discussion started: 13 December 2024

2.5 Deriving the Aerosol, CCN, and INP Vertical Profiles

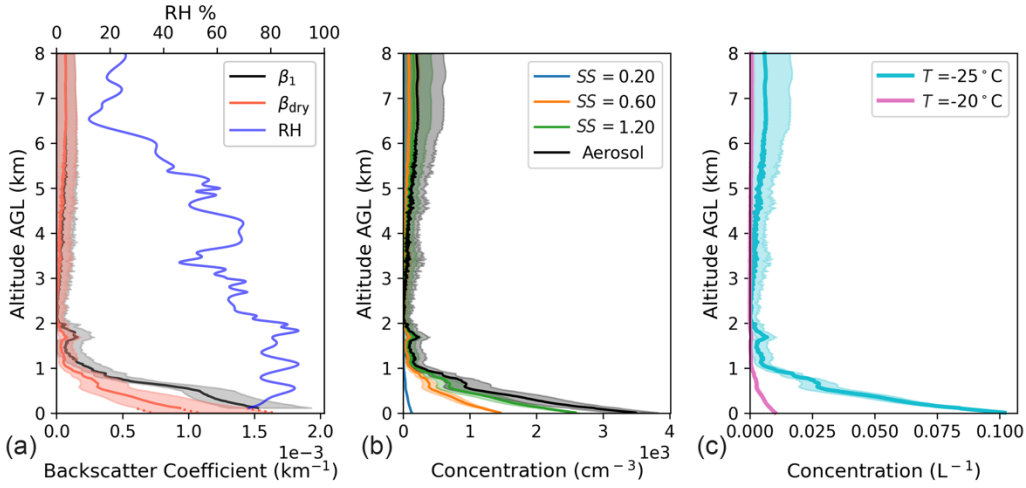

Figure 7 (a) Aerosol and dry aerosol backscatter coefficient profiles are shown as solid black and red lines, respectively, with a shaded area showing the corresponding uncertainty interval for each profile. The relative humidity profile is shown as a solid blue line. (b) The Aerosol profile is shown as a solid black line. CCN profiles are shown in different colors corresponding to supersaturation levels of 0.2%, 0.6%, and 1.2%. (c) INP profiles evaluated at -20°C and -25°C.

Based on the analysis above, we can now derive detailed vertical profiles of aerosol, CCN, and INP concentrations observed during the TRACER campaign. Here we assume that the surface measurements are representative of the aerosol size distribution, composition, and cloud-activating ability aloft. A caveat of this approach is that it holds true to well-mixed layers but cannot be used in cases in which layers of transported smoke or dust are observed in the NRB. The aerosol backscatter coefficient profile is shown in Figure 7a in a black line with a grey-shaded region as the uncertainty range. The dry aerosol backscatter coefficient profile $\beta_{\mathrm{dry}}(R)$ is

$$\beta_{\mathrm{dry}}(R) = \frac{\beta_1(R)}{f(RH)} \tag{7}$$

The RH profile is shown in Figure 7a with a solid blue line. The dry aerosol backscatter coefficient is shown in the red line with the red-shaded region as the uncertainty range. The lidar hygroscopic growth correction factor f(RH) uncertainty is considered and added to the uncertainties when calculating the dry

https://doi.org/10.5194/egusphere-2024-3363
Preprint. Discussion started: 13 December 2024

aerosol backscatter coefficient. The aerosol (N_p), CCN (N_{CCN}), and INP (N_{INP}) concentration profiles can therefore be estimated as:

$$N_{\mathrm{p}}(R) = \frac{\beta_{\mathrm{dry}}(R)}{\beta_{\mathrm{dry}}(R_0)} \cdot N_{\mathrm{p}}(R_0) \tag{8a}$$

$$N_{\mathrm{CCN}}(R, SS) = \frac{\beta_{\mathrm{dry}}(R)}{\beta_{\mathrm{dry}}(R_0)} \cdot N_{\mathrm{CCN}}(R_0, SS) \tag{8b}$$

$$N_{\mathrm{INP}}(R, T) = \frac{\beta_{\mathrm{dry}}(R)}{\beta_{\mathrm{dry}}(R_0)} \cdot N_{\mathrm{INP}}(R_0, T) \tag{8c}$$

R_0 is the altitude where the surface measurements are collected. $\beta_{\mathrm{dry}}(R_0)$ is the dry aerosol backscatter coefficient profile at R_0. N_{p}, N_{CCN}, and N_{INP} are aerosol, CCN, and INP number concentrations, respectively. Since the MPL and the MiniMPL have near-field blind ranges of 250 m and 100 m, respectively, lidar measurements near the surface are unavailable. A second-degree polynomial fitting of the dry aerosol backscatter coefficient profile from the lidar blind range to 300 m above is used to estimate the dry aerosol backscatter coefficient profile down to R_0, which is assumed to be around 10 m. The projected dry aerosol backscatter coefficient profiles within the blind range are shown in Figure 7a as dotted lines. The SS is the supersaturation at which the CCN concentration is evaluated, and T is the temperature at which the INP concentration is evaluated. In addition, one standard error of the time-averaged aerosol and CCN concentration of the time averaging period around 1 to 3 hours is included in the calculation for aerosol and CCN concentration profiles. The aerosol and CCN concentrations evaluated at different supersaturations are shown in Figure 7b. INP profiles are shown in Figure 7c. The dry aerosol backscatter coefficient profile determines the shape of aerosol, CCN, and INP concentration profiles, while the surface aerosol measurements determine the amplitude.

https://doi.org/10.5194/egusphere-2024-3363
Preprint. Discussion started: 13 December 2024

3 Results

3.1 Case study: Correction for Hygroscopic Growth in the Boundary Layer

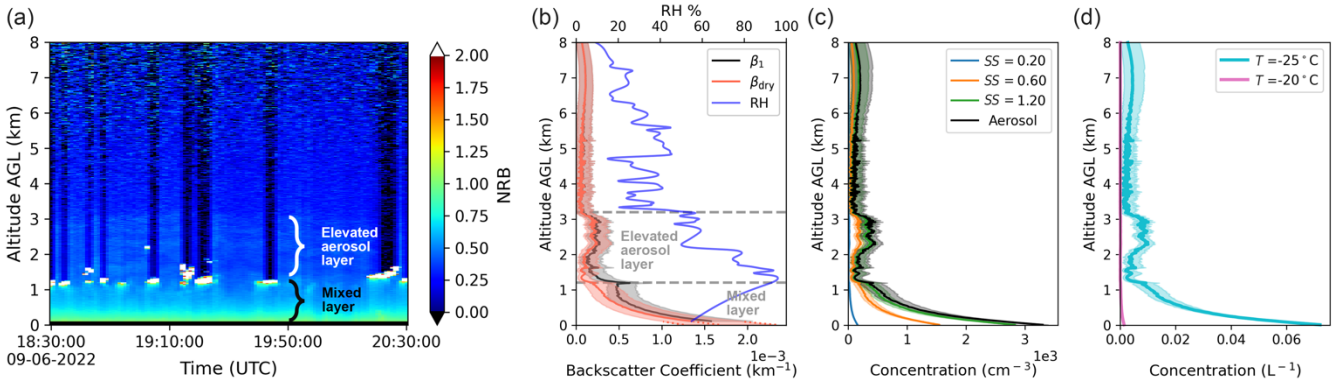

Figure 8 (a) NRB time series data collected on 6 September 2022, from 18:30 to 20:30 UTC, with MiniMPL inland at Hockley, Texas. (b) Aerosol and dry aerosol backscatter coefficient profiles are shown as solid black and red lines, respectively, with a shaded area showing the corresponding uncertainty interval for each profile. The relative humidity profile is shown as a solid blue line. (c) The Aerosol profile is shown as a solid black line. CCN profiles are shown in different colors corresponding to supersaturation levels of 0.2%, 0.6%, and 1.2%. (d) INP profiles evaluated at -20°C and -25°C. No INP was observed at -15°C.

An example from the measurements collected on 6 September 2022, during the inland TAMU deployment at Hockley, Texas, from 18:30 to 20:30 UTC, illustrates the importance of correcting for aerosol hygroscopic growth. Figure 8a shows the lidar NRB time-series profile. The layer at and below the cloud level height can be identified as a convective mixed layer, while the layer above the cloud level can be identified as an elevated aerosol layer. The cloud mask, which marks the temporal and vertical distribution of the cloud, is shown in Fig S2. The cloud mask was used to select a cloud-free lidar profile for aerosol backscatter coefficient profile retrieval. Figure 8b shows the cloud-free aerosol backscatter coefficient and the dry aerosol backscatter profile corrected for the water uptake by aerosols as RH increases. As the RH increases and approaches 100% in the mixed layer, the dry aerosol backscatter coefficient corrects for the increased backscatter due to aerosol growth. As Fig 8b demonstrates, if the uncorrected aerosol backscatter coefficient were used to estimate aerosol concentration in the mixed layer instead of the dry aerosol backscatter coefficient, the aerosol concentration would be substantially overestimated. For instance, relying on the uncorrected aerosol backscatter coefficient would result in an overestimation of

https://doi.org/10.5194/egusphere-2024-3363
Preprint. Discussion started: 13 December 2024

aerosol concentration by a factor of 2.8 at 1.2 km AGL. The aerosol concentration at the surface is approximately (3.30±0.09)×10^3 cm^{-3} and decreases to 371±216 cm^{-3} at the top of the mixed layer at 1.2 km AGL. The CCN concentration evaluated at a supersaturation of 0.2% is 159±2 cm^{-3} the at surface and 18±10 cm^{-3} at 1.2 km AGL (Figure 8d). The INP concentration evaluated at -20°C is around 0.07 L^{-1} at surface level and around 3×10^{-3} L^{-1} at 1 km AGL. No INP was observed at -15°C. Between 1.2 and 3.2 km, the dry aerosol backscatter coefficient profile indicates the presence of an elevated aerosol layer above the mixed layer. The aerosol population in the mixed layer and the elevated aerosol layer may differ in terms of aerosol size distribution and chemical composition, making this method for retrieving aerosol, CCN, and INP profiles more uncertain in the elevated aerosol layer shown in Figure 8.

3.2 Case study: Retrieval of Aerosol Profile with Multiple Cloud Layers

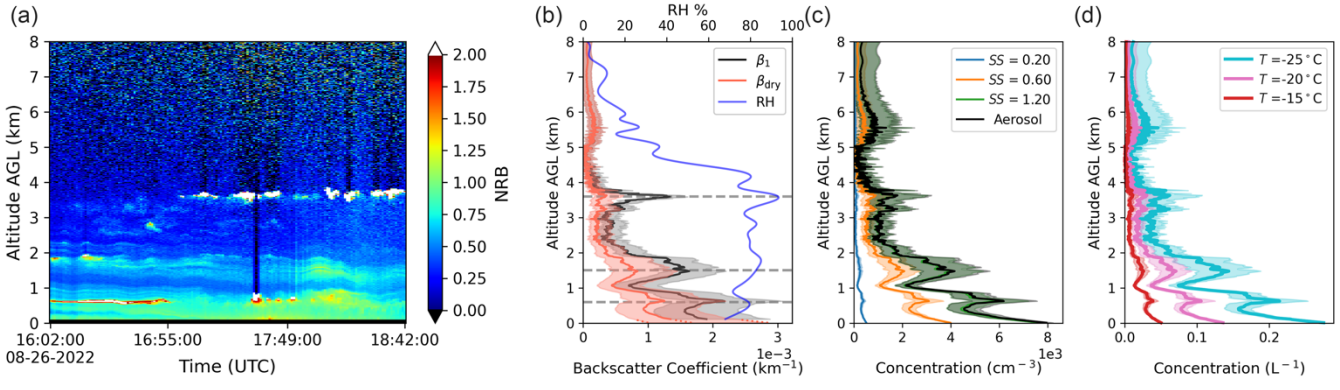

Figure 9 (a) NRB time series collected on 26 August 2022, from 16:02 to 18:42 UTC, with MiniMPL in Galveston, Texas. (b) Aerosol and dry aerosol backscatter coefficient profiles are shown as solid black and red lines, respectively, with a shaded area showing the corresponding uncertainty interval for each profile. The relative humidity profile is shown as a solid blue line. Gray dashed lines demonstrate the cloud level. (c) The Aerosol profile is shown as a solid black line. CCN profiles are shown in different colors corresponding to supersaturation levels of 0.2%, 0.6%, and 1.2%. (d) INP profiles at -15°C, -20°C and -25°C.

The next example, from the measurements collected on 26 August 2022 during the coastal TAMU deployment in Galveston, Texas, demonstrates the aerosol profile retrieval in the presence of multiple cloud layers. In Figure 9a, cloud layers around 0.6, 1.5, and 3.6 km can be identified as white pixels with high NRB. These cloud layers also match vertical regions of increased RH measured by the radiosonde launched around 17:26 UTC (Fig. 9b). A peak in the aerosol backscatter coefficient profile is seen around

https://doi.org/10.5194/egusphere-2024-3363
Preprint. Discussion started: 13 December 2024

3.6 km, showing a region where aerosol uptake water and grow in size (Fig. 9b). This peak is almost completely removed in the dry aerosol backscatter coefficient profile in Figure 9b, indicating a successful correction for the hygroscopic growth effect on aerosol scattering. This result also demonstrates that the lidar hygroscopic growth correction factor derived from surface measurements can also be applied to aerosol aloft. Increased aerosol backscatter coefficients around 0.6 and 1.5 km due to hygroscopic growth are also reduced, showing an expected aerosol vertical distribution. The results indicate that, at the surface level, the aerosol concentration is (7.95±0.27)×10^3 cm^{-3}, and it decreases by approximately 28% at 0.6 km, 50% at 1.5 km, and 79% at 3.6 km. At a supersaturation of 0.2%, the CCN concentrations are 511±10 cm^{-3} at the surface, 368±73 cm^{-3} at 0.6 km, 256±86 cm^{-3} at 1.5 km, and 107±82 cm^{-3} at 3.6 km. At a temperature of -15°C, the INP concentrations are around 0.05 L^{-1} at the surface, 0.04 L^{-1} at 0.6 km, 0.03 L^{-1} at 1.5 km, and 0.01 L^{-1} at 3.6 km. The correction for the aerosol hygroscopic growth leads to the more realistic aerosol, CCN, and INP profiles shown in Figure 8c, d, and Figure 9c, d.

3.3 Case study: Aerosol Profile under Clear Sky Conditions

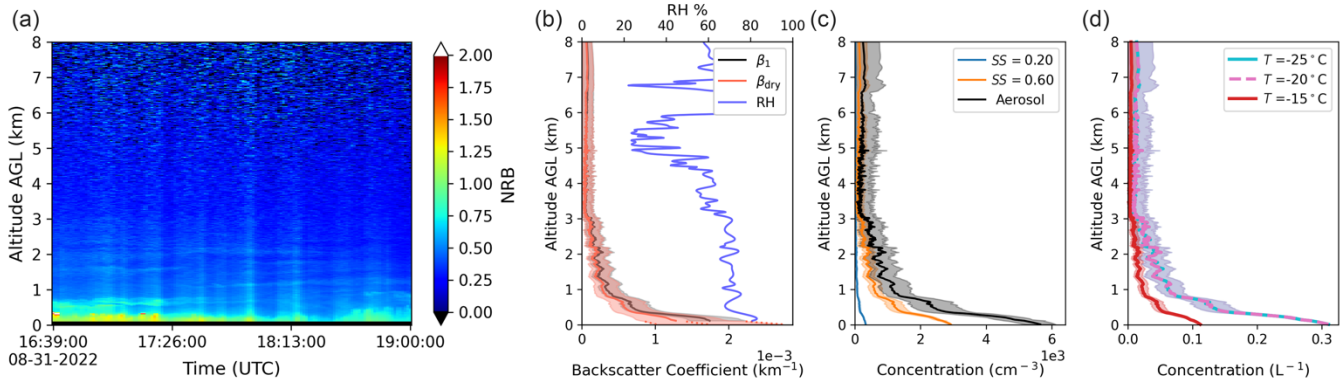

Figure 10 (a) NRB time series data collected on 31 August 2022, from 16:39 to 19:00 UTC, with MiniMPL in Galveston, Texas. (b) Aerosol and dry aerosol backscatter coefficient profiles are shown as solid black and red lines, respectively, with a shaded area showing the corresponding uncertainty interval for each profile. The relative humidity profile is shown as a solid blue line. Gray dashed lines demonstrate the cloud level. (c) The Aerosol profile is shown as a solid black line. CCN profiles are shown in different colors corresponding to supersaturation levels of 0.2% and 0.6%. CCN data for 1.2% supersaturation was not available. (d) INP profiles at -15°C, -20°C and -25°C. Note that the -20°C INP profile overlaps with the -25°C INP profile.

https://doi.org/10.5194/egusphere-2024-3363
Preprint. Discussion started: 13 December 2024

Measurements collected on 31 August 2022, in Galveston, Texas, from 16:39 to 19:00 UTC by MiniMPL show clear sky conditions in Figure 10a. One of the highest INP concentrations at -15 °C during the TRACER campaign was measured during this deployment. The RH profile is relatively stable below 8 km, at approximately 70%, and the hygroscopicity parameter κ is small, around $0.09 \times 2.70^{\pm1}$. As expected, with a constant RH profile and in the absence of distinct aerosol layers, the shape of the dry aerosol backscatter coefficient profile closely resembles that of the aerosol backscatter coefficient profile. The aerosol concentration near the surface and at 1 km are $(5.65\pm0.46)\times10^3$ cm^{-3} and $(1.14\pm0.57)\times10^3$ cm^{-3}. At a supersaturation of 0.2%, the CCN concentrations near the surface and at 1 km are approximately 329±2 cm^{-3} and 67±26 cm^{-3}. At a temperature of -15°C, the INP concentrations near the surface and at 1 km are approximately 0.11 L^{-1} and 0.02 L^{-1}.

3.4 Comparison Between Collocated MPL and MiniMPL Lidar

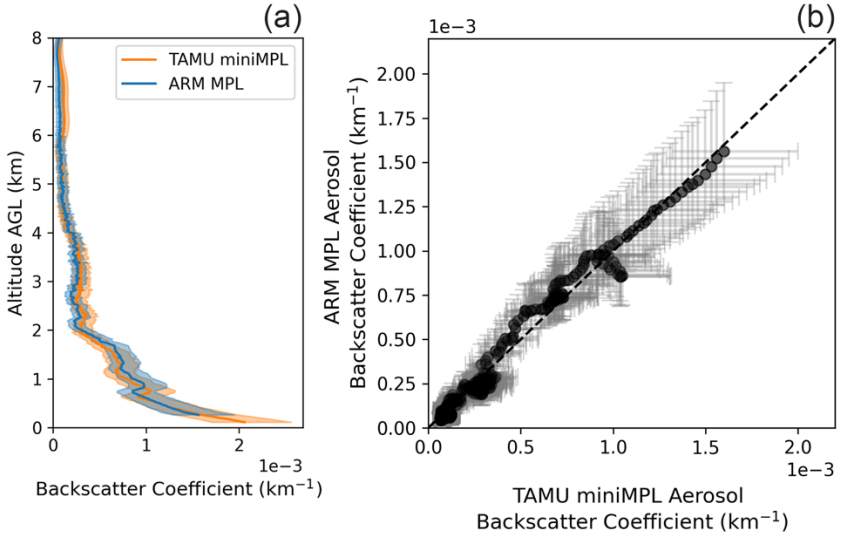

Figure 11 Comparison of retrieved aerosol backscatter coefficient profiles derived from MiniMPL and ARM AMF-1 MPL data. (a) MiniMPL aerosol backscatter coefficient profile is shown in a solid orange line, and the ARM AMF-1 MPL aerosol backscatter coefficient profile is shown in a blue line. Shaded areas show the corresponding uncertainty interval for each profile. (b) Comparison of the lidar aerosol backscatter coefficients interpolated to the same range. The uncertainty interval is shown as error bars.

https://doi.org/10.5194/egusphere-2024-3363
Preprint. Discussion started: 13 December 2024

The TAMU ROAM-V was deployed at the AMF1 (LaPorte, Texas) site on 1 September 2022, allowing MiniMPL and MPL to be collocated and compared directly. The ARM MPL deployed at AMF-1 collects data at a vertical resolution of 15 m and a temporal resolution of 10 s (Muradyan, 2021). The NRB data of both lidars are time-averaged between 20:00 and 22:00 UTC. The aerosol backscatter coefficient profiles are calculated following our method and shown in Figure 11a and 11b. The MPL and MiniMPL aerosol backscatter coefficient profiles follow similar shapes and magnitudes. The MiniMPL aerosol backscatter coefficients are slightly lower below 2 km, and there also seems to be a slight vertical misalignment below the 2 km. However, most of the differences between the two profiles are within the uncertainty ranges. The results show that following our method of smoothing the NRB and retrieving the aerosol backscatter coefficient, MiniMPL and MPL perform similarly despite the differences in the lidar designs and specifications. This agreement suggests that the MiniMPL, despite being a more compact and cost-effective option, can provide comparable data quality to the more established MPL system, and the retrieval results using both lidars can be compared directly.

3.5 Comparison between Aerosol and Cloud Condensation Nuclei Profiles at Galveston and LaPorte, TX measurements on 28 August 2022

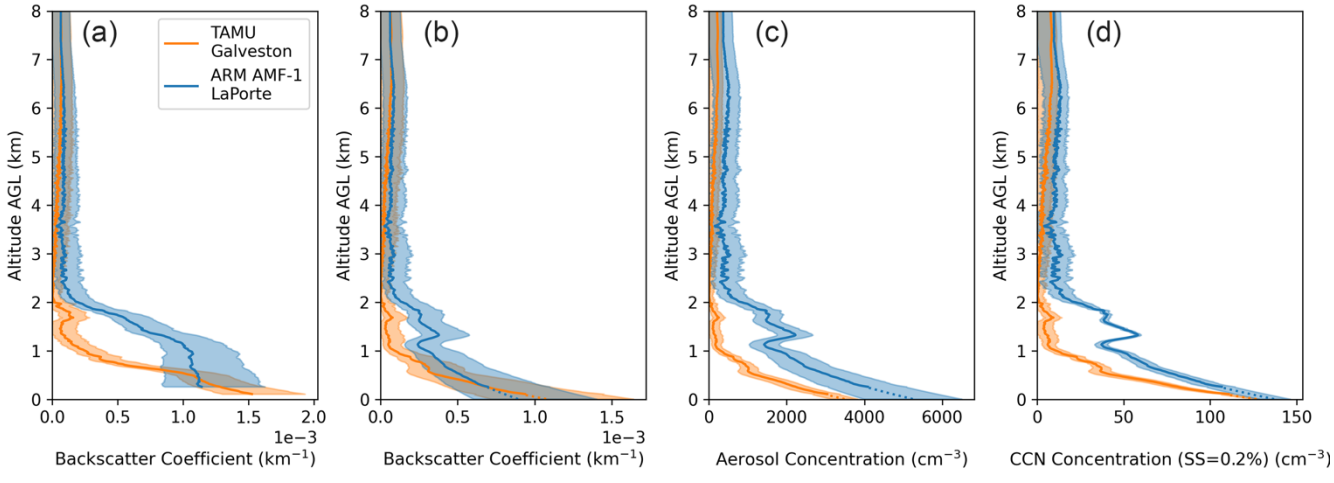

Figure 12 Comparison of lidar measurement of MiniMPL deployed at TAMU Galveston site and MPL deployed at ARM AMF-1 site on 28 August 2022, from 16:10 to 18:50 UTC (a) Aerosol backscatter coefficient profiles (b) Dry aerosol backscatter coefficient profiles (c) Aerosol concentration profile (d) CCN concentration profiles at 0.2% supersaturation.

https://doi.org/10.5194/egusphere-2024-3363
Preprint. Discussion started: 13 December 2024

A comparison between MiniMPL and ARM MPL measurements at different locations at the same time on 28 August 2022 is shown in Figure 12. MiniMPL was deployed at Sea Wolf Park, Galveston, Texas, and the AMF-1 was located in LaPorte, Texas. The straight-line distance is about 46 km. The time-averaging period was from 16:10 to 18:50 UTC. As shown in Figure 12b, near the ground surface, the dry aerosol backscatter coefficient near the surface at the 2 sites are similar. The dry aerosol backscatter coefficient at the TAMU Galveston site near the surface is $(1.07\pm0.57)\times10^3$ km^{-1}, and at the AMF-1 LaPorte site, it is $(0.89\pm0.51)\times10^3$ km^{-1}. The dry aerosol backscatter coefficient is greater at the AMF-1 LaPorte site at higher altitudes. Figure 12c and d show that the aerosol and CCN (SS = 0.2%) concentration at the AMF-1 LaPorte site is consistently greater than at the TAMU Galveston site at all vertical levels. At the surface, the aerosol concentration is $(3.49\pm0.34)\times10^3$ cm^{-3} for the TAMU site and $(5.24\pm1.26)\times10^3$ cm^{-3} for the ARM site. At 1 km altitude, these concentrations are 313±169 cm^{-3} and $(1.78\pm0.47)\times10^3$ cm^{-3} for the TAMU and ARM sites, respectively. In terms of CCN concentrations evaluated at 0.2% SS, at the surface, the TAMU site has a CCN concentration evaluated at 0.2% supersaturation of 127±2 cm^{-3}, while the ARM site has a slightly greater concentration of 137±9 cm^{-3}. At 1 km altitude, the CCN concentration at the TAMU site is 11±5 cm^{-3}, compared to a substantially greater concentration of 46±5 cm^{-3} at the ARM site.

These differences highlight variations in aerosol and CCN distributions between the two locations, especially at upper altitudes. The LaPorte site likely has a greater dry aerosol backscatter coefficient and aerosol concentration due to surrounding industrial emissions, while the TAMU Galveston site is more influenced by the maritime air mass. Despite similar surface aerosol and CCN number concentrations, there are clear differences in the aerosol and CCN vertical distribution between the two sites, only about 46 km apart. Such variability underscores the importance of localized aerosol vertical profile measurements in accurately characterizing aerosol vertical distributions when assessing their impact on air quality, weather, and climate. It also highlights the necessity of deploying multiple measurement sites to capture the spatial heterogeneity of aerosol vertical profiles when conducting a field campaign that covers a large study area, especially in regions influenced by heterogeneous sources of emissions and complex airmass interactions.

https://doi.org/10.5194/egusphere-2024-3363
Preprint. Discussion started: 13 December 2024

4 Discussions and Conclusions

This work uses data collected during the TRACER campaign to demonstrate a new method of retrieving aerosol, CCN, and INP profiles by integrating micropulse lidar measurements with radiosonde and ground-based aerosol measurements, including aerosol size distributions, CCN activation, and ice nucleation measurements. In the future, these measurements can be collected routinely to translate lidar backscatter coefficient profiles to long-term aerosol, CCN, and INP vertical profiles. Further, our method is not limited to the micropulse lidar and can be applied to other single-wavelength elastic or more advanced lidars.

One of the key findings of this study is that correcting aerosol hygroscopic growth is necessary for retrieving accurate CCN and INP concentration profiles. We have shown that using lidar-retrieved backscatter or extinction profiles without correcting for hygroscopic growth can lead to a significant overestimate of the aerosol concentration near the cloud base. To solve this issue, we introduced a method to quantify aerosol scattering enhancement due to aerosol hygroscopic growth. This method for determining the lidar hygroscopic growth correction factor can be used as a complementary approach to the traditional method of using a collocated humidified nephelometer (Ghan et al., 2006) and can be used when a humidified nephelometer is unavailable.

Another key finding is that aerosol and CCN vertical distributions can significantly vary at small spatial scales, even when similar aerosol and CCN concentrations are collected at the surface, as demonstrated by the comparison between the aerosol vertical profile at ARM and TAMU site on 28 August 2022. This variability highlights the importance of considering vertical profiles rather than relying solely on ground based aerosol measurements when assessing aerosol properties and their impacts on cloud formation. It also underscores the need for localized vertical profile measurements to accurately capture the diverse aerosol characteristics in different regions, particularly in areas with complex emission sources and air mass interactions. Portable lidars, such as the MiniMPL lidar, combined with surface aerosol measurements, can be highly effective in providing these localized aerosol vertical profile measurements.

https://doi.org/10.5194/egusphere-2024-3363
Preprint. Discussion started: 13 December 2024

While the method described herein clearly has some distinct advantages, it is subject to several limitations. Since the MPL and MiniMPL measurements are noisy at upper altitudes, this method's retrieval above the altitude where the lidar signal is smoothed should be used with caution and can only serve as a best estimate. In addition, since our method relies on the assumption that the aerosol size distribution and composition are similar throughout the vertical column, the retrieved profiles are the most reliable within the well-mixed boundary layer. At altitudes where aerosol properties differ significantly from those at the surface, such as in the presence of a transported dust layer in the free troposphere, this method may be less reliable, and the results should be interpreted with caution. Despite these limitations, as measurements of CCN and INP vertical profiles are difficult to obtain and sparse, the results from this method can serve as a significant improvement over the arbitrary aerosol profiles often used in model initialization.

In conclusion, the integration of micropulse lidar and ground-based aerosol measurements offers a powerful tool for retrieving detailed vertical profiles of aerosols, CCN, and INPs. The retrieved profiles can serve as inputs to provide realistic aerosol vertical distributions for cloud-resolving models, facilitating the study of aerosol-cloud interactions and aerosol effects on climate.

https://doi.org/10.5194/egusphere-2024-3363
Preprint. Discussion started: 13 December 2024

5 Author Contribution

S.D. Brooks conceived of the project. B.C. and S.D. Brooks designed the analysis and lead the writing of the manuscript. B.C., S.A.T., B.H.M., and R.L. collected and curated the data. M.S. C.J.N. and A.D.R. contributed to the data interpretation and writing of the manuscript.

6 Data Availability

The data used in this analysis is available in the DOE ARM data archive: https://adc.arm.gov//discovery/#/results/site_code::hou.

7 Competing Interest

The authors declare that they have no conflict of interest.

8 Acknowledgement

This research was funded by the U.S. Department of Energy's Atmospheric System Research (DOE ASR) Program under award #DE-SC0021047.

References

Albrecht, B. A.: Aerosols, cloud microphysics, and fractional cloudiness, Science, 245, 1227-1230, 1989.
Andreae, M. O., Rosenfeld, D., Artaxo, P., Costa, A. A., Frank, G., Longo, K. M., and Silva-Dias, M. A. F. d.: Smoking rain clouds over the Amazon, science, 303, 1337-1342, 2004.
Ansmann, A., Ohneiser, K., Mamouri, R.-E., Knopf, D. A., Veselovskii, I., Baars, H., Engelmann, R., Foth, A., Jimenez, C., and Seifert, P.: Tropospheric and stratospheric wildfire smoke profiling with lidar: mass, surface area, CCN, and INP retrieval, Atmospheric Chemistry and Physics, 21, 9779-9807, 2021.
Brooks, S. and Chen, B.: Mini-Micropulse Lidar data from TAMU TRACER campaign in the Houston TX region from July to September 2022, Oak Ridge National Lab.(ORNL), Oak Ridge, TN (United States). Atmospheric …, 2023.
Brooks, S. and Thompson, S.: Ice nucleation measurements from DRUM impactors during TRACER campaign in the Houston TX region from July to September 2022, Oak Ridge National Lab.(ORNL), Oak Ridge, TN (United States). Atmospheric …, 2023.
Brooks, S. D., DeMott, P. J., and Kreidenweis, S. M.: Water uptake by particles containing humic materials and mixtures of humic materials with ammonium sulfate, Atmospheric Environment, 38, 1859-1868, 2004a.
Brooks, S. D., Toon, O. B., Tolbert, M. A., Baumgardner, D., Gandrud, B. W., Browell, E. V., Flentje, H., and Wilson, J. C.: Polar stratospheric clouds during SOLVE/THESEO: Comparison of lidar observations with in situ measurements, Journal of Geophysical Research: Atmospheres, 109, 2004b.
Cai, T. T. and Silverman, B. W.: Incorporating information on neighbouring coefficients into wavelet estimation, Sankhyā: The Indian Journal of Statistics, Series B, 127-148, 2001.

https://doi.org/10.5194/egusphere-2024-3363
Preprint. Discussion started: 13 December 2024

Campbell, J. R., Hlavka, D. L., Welton, E. J., Flynn, C. J., Turner, D. D., Spinhirne, J. D., Scott III, V. S., and Hwang, I.: Full-time, eye-safe cloud and aerosol lidar observation at atmospheric radiation measurement program sites: Instruments and data processing, Journal of Atmospheric and Oceanic Technology, 19, 431-442, 2002.

Chen, B., Thompson, S. A., and Brooks, S. D.: TAMU TRACER SMPS-POPS Merged Size Distribution (V1), Texas Data Repository [dataset], doi/10.18738/T8/NUX5AZ, 2024.

Cotterell, M. I., Willoughby, R. E., Bzdek, B. R., Orr-Ewing, A. J., and Reid, J. P.: A complete parameterisation of the relative humidity and wavelength dependence of the refractive index of hygroscopic inorganic aerosol particles, Atmospheric Chemistry and Physics, 17, 9837-9851, 2017.

Dadashazar, H., Crosbie, E., Choi, Y., Corral, A. F., DiGangi, J. P., Diskin, G. S., Dmitrovic, S., Kirschler, S., McCauley, K., and Moore, R. H.: Analysis of MONARC and ACTIVATE Airborne Aerosol Data for Aerosol-Cloud Interaction Investigations: Efficacy of Stairstepping Flight Legs for Airborne In Situ Sampling, Atmosphere, 13, 1242, 2022.

DeMott, P. J., Prenni, A. J., Liu, X., Kreidenweis, S. M., Petters, M. D., Twohy, C. H., Richardson, M., Eidhammer, T., and Rogers, D.: Predicting global atmospheric ice nuclei distributions and their impacts on climate, Proceedings of the National Academy of Sciences, 107, 11217-11222, 2010.

DeMott, P. J., Prenni, A. J., McMeeking, G. R., Sullivan, R. C., Petters, M. D., Tobo, Y., Niemand, M., Möhler, O., Snider, J. R., and Wang, Z.: Integrating laboratory and field data to quantify the immersion freezing ice nucleation activity of mineral dust particles, Atmospheric Chemistry and Physics, 15, 393-409, 2015.

Du, P., Kibbe, W. A., and Lin, S. M.: Improved peak detection in mass spectrum by incorporating continuous wavelet transform-based pattern matching, bioinformatics, 22, 2059-2065, 2006.

Fan, J., Wang, Y., Rosenfeld, D., and Liu, X.: Review of aerosol–cloud interactions: Mechanisms, significance, and challenges, Journal of the Atmospheric Sciences, 73, 4221-4252, 2016.

Fan, J., Zhang, R., Li, G., and Tao, W. K.: Effects of aerosols and relative humidity on cumulus clouds, Journal of Geophysical Research: Atmospheres, 112, 2007.

Fan, J., Rosenfeld, D., Zhang, Y., Giangrande, S. E., Li, Z., Machado, L. A., Martin, S. T., Yang, Y., Wang, J., and Artaxo, P.: Substantial convection and precipitation enhancements by ultrafine aerosol particles, Science, 359, 411-418, 2018.

Fang, H.-T. and Huang, D.-S.: Noise reduction in lidar signal based on discrete wavelet transform, Optics Communications, 233, 67-76, 2004.

Fernald, F. G.: Analysis of atmospheric lidar observations: some comments, Applied optics, 23, 652-653, 1984.

Fernald, F. G., Herman, B. M., and Reagan, J. A.: Determination of aerosol height distributions by lidar, Journal of Applied Meteorology and Climatology, 11, 482-489, 1972.

Flynna, C. J., Mendozaa, A., Zhengb, Y., and Mathurb, S.: Novel polarization-sensitive micropulse lidar measurement technique, Optics express, 15, 2785-2790, 2007.

Fornea, A. P., Brooks, S. D., Dooley, J. B., and Saha, A.: Heterogeneous freezing of ice on atmospheric aerosols containing ash, soot, and soil, Journal of Geophysical Research: Atmospheres, 114, 2009.

Ghan, S. J. and Collins, D. R.: Use of in situ data to test a Raman lidar–based cloud condensation nuclei remote sensing method, Journal of Atmospheric and Oceanic Technology, 21, 387-394, 2004.

Ghan, S. J., Rissman, T. A., Elleman, R., Ferrare, R. A., Turner, D., Flynn, C., Wang, J., Ogren, J., Hudson, J., and Jonsson, H. H.: Use of in situ cloud condensation nuclei, extinction, and aerosol size distribution measurements to test a method for retrieving cloud condensation nuclei profiles from surface measurements, Journal of Geophysical Research: Atmospheres, 111, 2006.

Gimmestad, G. G. and Roberts, D. W.: Lidar engineering: introduction to basic principles, Cambridge University Press2023.

Igel, A. L. and van den Heever, S. C.: Invigoration or enervation of convective clouds by aerosols?, Geophysical Research Letters, 48, e2021GL093804, 2021.

Jensen, M.: Tracking Aerosol Convection Interactions Experiment (TRACER) Field Campaign Report, Oak Ridge National Laboratory (ORNL), Oak Ridge, TN (United States …, 2023.

Kapustin, V., Clarke, A., Shinozuka, Y., Howell, S., Brekhovskikh, V., Nakajima, T., and Higurashi, A.: On the determination of a cloud condensation nuclei from satellite: Challenges and possibilities, Journal of Geophysical Research: Atmospheres, 111, 2006.

Keeler, E., Burk, K., and Kyrouac, J.: Balloon-Borne Sounding System (SONDEWNPN) [dataset], http://dx.doi.org/10.5439/1595321., 2021.

https://doi.org/10.5194/egusphere-2024-3363
Preprint. Discussion started: 13 December 2024

Klett, J. D.: Stable analytical inversion solution for processing lidar returns, Applied optics, 20, 211-220, 1981.
Koontz, A., Uin, J., Andrews, E., Enekwizu, O., Hayes, C., and Salwen, C.: Cloud Condensation Nuclei Particle Counter (AOSCCN2COLASPECTRA) [dataset], https://doi.org/10.5439/1323896, 2021.
Kotchenruther, R. A., Hobbs, P. V., and Hegg, D. A.: Humidification factors for atmospheric aerosols off the mid-Atlantic coast of the United States, Journal of Geophysical Research: Atmospheres, 104, 2239-2251, 1999.
Kulkarni, G., Sivaraman, C., and Shilling, J.: Retrieved Number Concentration of Cloud Condensation Nuclei (RNCCN) Profile Value-Added Product Report, Oak Ridge National Laboratory (ORNL), Oak Ridge, TN (United States …, 2023.
Lebo, Z.: A numerical investigation of the potential effects of aerosol-induced warming and updraft width and slope on updraft intensity in deep convective clouds, Journal of the Atmospheric Sciences, 75, 535-554, 2018.
Lebo, Z. and Seinfeld, J.: Theoretical basis for convective invigoration due to increased aerosol concentration, Atmospheric Chemistry and Physics, 11, 5407-5429, 2011.
Lebo, Z. J.: The sensitivity of a numerically simulated idealized squall line to the vertical distribution of aerosols, Journal of the Atmospheric Sciences, 71, 4581-4596, 2014.
Lei, Z., Chen, B., and Brooks, S. D.: Effect of acidity on ice nucleation by inorganic–organic mixed droplets, ACS Earth and Space Chemistry, 7, 2562-2573, 2023.
Lenhardt, E. D., Gao, L., Redemann, J., Xu, F., Burton, S. P., Cairns, B., Chang, I., Ferrare, R. A., Hostetler, C. A., and Saide, P. E.: Use of lidar aerosol extinction and backscatter coefficients to estimate cloud condensation nuclei (CCN) concentrations in the southeast Atlantic, Atmospheric Measurement Techniques, 16, 2037-2054, 2023.
Lin, Y., Takano, Y., Gu, Y., Wang, Y., Zhou, S., Zhang, T., Zhu, K., Wang, J., Zhao, B., and Chen, G.: Characterization of the aerosol vertical distributions and their impacts on warm clouds based on multi-year ARM observations, Science of The Total Environment, 904, 166582, 2023.
Liu, J. and Li, Z.: Estimation of cloud condensation nuclei concentration from aerosol optical quantities: influential factors and uncertainties, Atmospheric Chemistry and Physics, 14, 471-483, 2014.
Lv, M., Wang, Z., Li, Z., Luo, T., Ferrare, R., Liu, D., Wu, D., Mao, J., Wan, B., and Zhang, F.: Retrieval of cloud condensation nuclei number concentration profiles from lidar extinction and backscatter data, Journal of Geophysical Research: Atmospheres, 123, 6082-6098, 2018.
Mamouri, R.-E. and Ansmann, A.: Potential of polarization lidar to provide profiles of CCN-and INP-relevant aerosol parameters, Atmospheric Chemistry and Physics, 16, 5905-5931, 2016.
Marinescu, P. J., van den Heever, S. C., Saleeby, S. M., Kreidenweis, S. M., and DeMott, P. J.: The microphysical roles of lower-tropospheric versus midtropospheric aerosol particles in mature-stage MCS precipitation, Journal of the Atmospheric Sciences, 74, 3657-3678, 2017.
Marinou, E., Tesche, M., Nenes, A., Ansmann, A., Schrod, J., Mamali, D., Tsekeri, A., Pikridas, M., Baars, H., and Engelmann, R.: Retrieval of ice-nucleating particle concentrations from lidar observations and comparison with UAV in situ measurements, Atmospheric Chemistry and Physics, 19, 11315-11342, 2019.
Müller, D., Kolgotin, A., Mattis, I., Petzold, A., and Stohl, A.: Vertical profiles of microphysical particle properties derived from inversion with two-dimensional regularization of multiwavelength Raman lidar data: experiment, Applied Optics, 50, 2069-2079, 2011.
Müller, D., Hostetler, C. A., Ferrare, R., Burton, S., Chemyakin, E., Kolgotin, A., Hair, J. W., Cook, A., Harper, D. B., and Rogers, R.: Airborne multiwavelength high spectral resolution lidar (HSRL-2) observations during TCAP 2012: vertical profiles of optical and microphysical properties of a smoke/urban haze plume over the northeastern coast of the US, Atmospheric measurement techniques, 7, 3487-3496, 2014.
Muradyan, P., Cromwell, E., Koontz, A., Coulter, R., Flynn, C., Ermold, B., and OBrien, J.: Micropulse Lidar (MPLPOLFS). [dataset], https://doi.org/10.5439/1320657, 2021.
Niemand, M., Möhler, O., Vogel, B., Vogel, H., Hoose, C., Connolly, P., Klein, H., Bingemer, H., DeMott, P., and Skrotzki, J.: A particle-surface-area-based parameterization of immersion freezing on desert dust particles, Journal of the Atmospheric Sciences, 69, 3077-3092, 2012.
Onasch, T. B., Siefert, R. L., Brooks, S. D., Prenni, A. J., Murray, B., Wilson, M. A., and Tolbert, M. A.: Infrared spectroscopic study of the deliquescence and efflorescence of ammonium sulfate aerosol as a function of temperature, Journal of Geophysical Research: Atmospheres, 104, 21317-21326, 1999.

https://doi.org/10.5194/egusphere-2024-3363
Preprint. Discussion started: 13 December 2024

Perkins, R. J., Marinescu, P. J., Levin, E. J., Collins, D. R., and Kreidenweis, S. M.: Long-and short-term temporal variability in cloud condensation nuclei spectra over a wide supersaturation range in the Southern Great Plains site, Atmospheric Chemistry and Physics, 22, 6197-6215, 2022.

Petters, M. and Kreidenweis, S.: A single parameter representation of hygroscopic growth and cloud condensation nucleus activity, Atmospheric Chemistry and Physics, 7, 1961-1971, 2007.

Pöhlker, M. L., Pöhlker, C., Ditas, F., Klimach, T., Hrabe de Angelis, I., Araújo, A., Brito, J., Carbone, S., Cheng, Y., and Chi, X.: Long-term observations of cloud condensation nuclei in the Amazon rain forest–Part 1: Aerosol size distribution, hygroscopicity, and new model parametrizations for CCN prediction, Atmospheric Chemistry and Physics, 16, 15709-15740, 2016.

Raes, F., Bates, T., McGOVERN, F., and Van Liedekerke, M.: The 2nd Aerosol Characterization Experiment (ACE-2): General overview and main results, Tellus B: Chemical and Physical Meteorology, 52, 111-125, 2000.

Rapp, A. D., Brooks, S. D., Nowotarski, C. J., Sharma, M., Thompson, S. A., Chen, B., Matthews, B. H., Etten-Bohm, M., Nielsen, E. R., and Li, R.: TAMU TRACER: Targeted Mobile Measurements to Isolate the Impacts of Aerosols and Meteorology on Deep Convection, Bulletin of the American Meteorological Society, 2024.

Rosenfeld, D., Lohmann, U., Raga, G. B., O'Dowd, C. D., Kulmala, M., Fuzzi, S., Reissell, A., and Andreae, M. O.: Flood or drought: how do aerosols affect precipitation?, science, 321, 1309-1313, 2008.

Rosenfeld, D., Andreae, M. O., Asmi, A., Chin, M., de Leeuw, G., Donovan, D. P., Kahn, R., Kinne, S., Kivekäs, N., and Kulmala, M.: Global observations of aerosol-cloud-precipitation-climate interactions, Reviews of Geophysics, 52, 750-808, 2014.

Sasano, Y., Browell, E. V., and Ismail, S.: Error caused by using a constant extinction/backscattering ratio in the lidar solution, Applied Optics, 24, 3929-3932, 1985.

Schmale, J., Henning, S., Decesari, S., Henzing, B., Keskinen, H., Sellegri, K., Ovadnevaite, J., Pöhlker, M. L., Brito, J., and Bougiatioti, A.: Long-term cloud condensation nuclei number concentration, particle number size distribution and chemical composition measurements at regionally representative observatories, Atmospheric Chemistry and Physics, 18, 2853-2881, 2018.

Seinfeld, J. H., Bretherton, C., Carslaw, K. S., Coe, H., DeMott, P. J., Dunlea, E. J., Feingold, G., Ghan, S., Guenther, A. B., and Kahn, R.: Improving our fundamental understanding of the role of aerosol− cloud interactions in the climate system, Proceedings of the National Academy of Sciences, 113, 5781-5790, 2016.

Sharma, M., Rapp, A., and Nowotarski, C.: TAMU TRACER Upper Air Radiosonde Data June-September 2022 Southeast Texas, Oak Ridge National Lab.(ORNL), Oak Ridge, TN (United States). Atmospheric …, 2023.

Shinozuka, Y., Clarke, A. D., Nenes, A., Jefferson, A., Wood, R., McNaughton, C. S., Ström, J., Tunved, P., Redemann, J., and Thornhill, K. L.: The relationship between cloud condensation nuclei (CCN) concentration and light extinction of dried particles: indications of underlying aerosol processes and implications for satellite-based CCN estimates, Atmospheric Chemistry and Physics, 15, 7585-7604, 2015.

Steinke, I., Hoose, C., Möhler, O., Connolly, P., and Leisner, T.: A new temperature-and humidity-dependent surface site density approach for deposition ice nucleation, Atmospheric Chemistry and Physics, 15, 3703-3717, 2015.

Stith, J., Ramanathan, V., Cooper, W., Roberts, G., DeMott, P., Carmichael, G., Hatch, C., Adhikary, B., Twohy, C., and Rogers, D.: An overview of aircraft observations from the Pacific Dust Experiment campaign, Journal of Geophysical Research: Atmospheres, 114, 2009.

Su, H., Rose, D., Cheng, Y., Gunthe, S., Massling, A., Stock, M., Wiedensohler, A., Andreae, M., and Pöschl, U.: Hygroscopicity distribution concept for measurement data analysis and modeling of aerosol particle mixing state with regard to hygroscopic growth and CCN activation, Atmospheric Chemistry and Physics, 10, 7489-7503, 2010.

Tao, W. K., Chen, J. P., Li, Z., Wang, C., and Zhang, C.: Impact of aerosols on convective clouds and precipitation, Reviews of Geophysics, 50, 2012.

Thompson, S. A., Brooks, Sarah D: CCN data from TAMU TRACER campaign in the Houston TX region from July to September 2022, DOE ARM Archive User Services [dataset], 10.5439/1972179, 2023.

Thompson, S. A., Chen, B., Matthews, B. H., Li, R., Nowotarski, C. J., Rapp, A. D., & Brooks, S. D.: Characterizing Greater Houston's aerosol by airmass during TRACER, Journal of Geophysical Research: Atmospheres, 2024.

https://doi.org/10.5194/egusphere-2024-3363
Preprint. Discussion started: 13 December 2024

Titos, G., Cazorla, A., Zieger, P., Andrews, E., Lyamani, H., Granados-Muñoz, M. J., Olmo, F., and Alados-Arboledas, L.: Effect of hygroscopic growth on the aerosol light-scattering coefficient: A review of measurements, techniques and error sources, Atmospheric Environment, 141, 494-507, 2016.

Tobo, Y., Prenni, A. J., DeMott, P. J., Huffman, J. A., McCluskey, C. S., Tian, G., Pöhlker, C., Pöschl, U., and Kreidenweis, S. M.: Biological aerosol particles as a key determinant of ice nuclei populations in a forest ecosystem, Journal of Geophysical Research: Atmospheres, 118, 10,100-110,110, 2013.

Tomlinson, J. M., Li, R., and Collins, D. R.: Physical and chemical properties of the aerosol within the southeastern Pacific marine boundary layer, Journal of Geophysical Research: Atmospheres, 112, 2007.

Twomey, S.: The influence of pollution on the shortwave albedo of clouds, Journal of the atmospheric sciences, 34, 1149-1152, 1977.

Ullrich, R., Hoose, C., Möhler, O., Niemand, M., Wagner, R., Höhler, K., Hiranuma, N., Saathoff, H., and Leisner, T.: A new ice nucleation active site parameterization for desert dust and soot, Journal of the Atmospheric Sciences, 74, 699-717, 2017.

Vali, G.: Quantitative evaluation of experimental results an the heterogeneous freezing nucleation of supercooled liquids, Journal of Atmospheric Sciences, 28, 402-409, 1971.

Varble, A. C., Igel, A. L., Morrison, H., Grabowski, W. W., and Lebo, Z. J.: Opinion: A critical evaluation of the evidence for aerosol invigoration of deep convection, Atmospheric Chemistry and Physics, 23, 13791-13808, 2023.

Wang, B. and Knopf, D. A.: Heterogeneous ice nucleation on particles composed of humic-like substances impacted by O3, Journal of Geophysical Research: Atmospheres, 116, 2011.

Welton, E. J. and Campbell, J. R.: Micropulse lidar signals: Uncertainty analysis, Journal of Atmospheric and Oceanic Technology, 19, 2089-2094, 2002.

Xie, H., Zhou, T., Fu, Q., Huang, J., Huang, Z., Bi, J., Shi, J., Zhang, B., and Ge, J.: Automated detection of cloud and aerosol features with SACOL micro-pulse lidar in northwest China, Optics Express, 25, 30732-30753, 2017.

Yao, Y., Curtis, J. H., Ching, J., Zheng, Z., and Riemer, N.: Quantifying the effects of mixing state on aerosol optical properties, Atmospheric Chemistry and Physics, 22, 9265-9282, 2022.

Young, S. A., Vaughan, M. A., Garnier, A., Tackett, J. L., Lambeth, J. D., and Powell, K. A.: Extinction and optical depth retrievals for CALIPSO's Version 4 data release, Atmospheric Measurement Techniques, 11, 5701-5727, 2018.

Zhang, M., Deng, X., Zhu, R., Ren, Y., and Xue, H.: The impact of aerosol vertical distribution on a deep convective cloud, Atmosphere, 12, 675, 2021.